Journal Name

ARTICLE

Room-Temperature Switching of Magnetic Hysteresis by Reversible Single-Crystal-to-Single-Crystal Solvent Exchange in Imidazole-Inspired Fe(II) Complex

Received 00th January 20xx,
Accepted 00th January 20xx

DOI: 10.1039/x0xx00000x

www.rsc.org/

Wei Huang,[a] Fuxing Shen,[a] Ming Zhang,[a] Dayu Wu,[a]* Feifei Pan,[a] and Osamu Sato[b]

The recent upsurge in molecular magnetism reflects their application in the areas of sensors and molecular switches. The thermal hysteresis is crucial to the molecular bistability and information storage, wide hysteresis near room temperature is expected to be of practical sense for the molecular compound. In this work, the spin crossover iron(II) complexes $[Fe(Liq)_2](BF_4)_2\cdot(CH_3CH_2)_2O$ (**1**-Et_2O) and $[Fe(Liq)_2](BF_4)_2\cdot 3H_2O$ (**1**-$3H_2O$) were prepared, structurally and magnetically analysed. The single-crystal-to-single-crystal (SCSC) solvation transformation and the influence on the crystal structures and magnetic hysteresis were investigated in etherification-hydration cycle. At room temperature, X-ray diffraction experiments indicated a transformation from one crystal (**1**-Et_2O, $P2_12_12$) to another crystal (**1**-$3H_2O$, $P2_12_12_1$) upon humidity exposure and reversible recovery of its crystallinity upon exposure to ether vapor. The etherified phase **1**-Et_2O exhibits room temperature spin crossover ($T_{1/2}$ = 305 K) but negligible thermal hysteresis, however, the hydrated phase **1**-$3H_2O$ exhibit the apparent hysteresis loop ($T_{1/2}\uparrow$ = 346K, $T_{1/2}\downarrow$ = 326 K) which expands to room temperature. This effect is associated with the change of intermolecular cooperativity in the etherification-hydration recyclability.

Introduction

The spin-crossover phenomenon (SCO) is a fascinating field that corresponds to the switching of the electronic configuration of a transition metal compound between high spin (HS) and low spin (LS) states as a result of an external perturbation, such as temperature, pressure, light irradiation, magnetic and electric fields.[1] Considerable efforts have been devoted to improving the performance of SCO materials in order to realize their applications as molecular switches, nano-sensors, data storage and display devices.[2,3] However, most SCO materials reported so far experience spin transitions (STs) at low temperatures rather than room temperature due to the thermal equilibrium between high spin (HS) and low spin (LS) state with moderate field ligand.[4] Fe(II) triazole complexes and Hoffman-type clathrates exhibit room-temperature (RT) hysteresis which is crucial to the application of information storage.[5,6] The nitrogen-rich chelates are known to act as intermediate-field ligands might open an access to obtain RT-operable switchable materials.[7,8] Grimme, Sarkar and coworkers reported the solvent-free Fe(II) complex based on ligand tris[(1-benzyl-1H-1,2,3-triazol-4-yl)methyl]amine (tbta) which displays spin crossover (SCO) with a spin transition temperature $T_{1/2}$ near room temperature.[9] Gao et al reported the solvent-sensitive spin crossover near room temperature by employing the N_4O_2-type coordination donor.[10] Hence, room temperature (around 300 K) SCO or ST compounds have been rarely reported so far due to the difficulty of the selecting the suitable ligand field strength, thermal instability and etc.[11] Especially, the compound with a wide thermal hysteresis at RT is important for practical applications.[12] Despite of many attempts made to prepare one compound in previous studies, the production of spin-crossover compounds with such a wide hysteresis at room temperature is still rare.[13] It is still a great challenge to design systems that can be tuned on purpose toward around RT spin transition, especially with wide hysteresis.

Another hot topic in the SCO field is to modulate the spin-state through host-guest sensing event, where effects of the guest molecules are mediated by van der Waals interactions, hydrogen bonds, π-π interactions, or structural changes.[14] Recent developments in this field have aimed at the incorporation of spin-crossover sites in 2D or 3D frameworks, which makes them interesting candidates for potential sensing applications.[15] In most cases, exposure to guest solvent molecules could induce or change the SCO properties of the host.[16] The systematic modification of the SCO properties, especially of the hysteresis near room temperature in the fashion of reversible single-crystal-to-single-crystal (SCSC) guest exchange, has been rarely investigated up to now.[17]

Here, we report the magnetostructural study on the solvate Fe(II) complex of formula $[Fe(Liq)_2](BF_4)_2\cdot(CH_3CH_2)_2O$ (denoted as 1-Et_2O)

[a] Jiangsu Key Laboratory of Advanced Catalytic Materials and Technology, School of Petrochemical Engineering, Changzhou University, Changzhou 213164, People's Republic of China.E-mail: wudy@cczu.edu.cn
[b] Institute for Materials Chemistry and Engineering, Kyushu University, 744 Motooka, Nishi-ku, Fukuoka, 819-0395, Japan.
† Footnotes relating to the title and/or authors should appear here.
Electronic Supplementary Information (ESI) available: [details of any supplementary information available should be included here]. See DOI: 10.1039/x0xx00000x

(Liq = 3-((1H-imidazol-4-yl)methyleneamino)-2,3-dihydro-2-(1H-imidazol-4-yl)quinazolin-4(1H)-one,[18] abbreviated as Liq, hereafter) which exhibits a spin crossover with $T_{1/2}$ around room temperature. The solvent-exchanged species, $[Fe(Liq)_2](BF_4)_2{\cdot}3H_2O$ (denoted as 1-$3H_2O$), was investigated to establish the hydration induced apparent hysteresis loops with ΔT = 20 K, which can be reversibly switched on/off by the etherification-hydration recyclability.

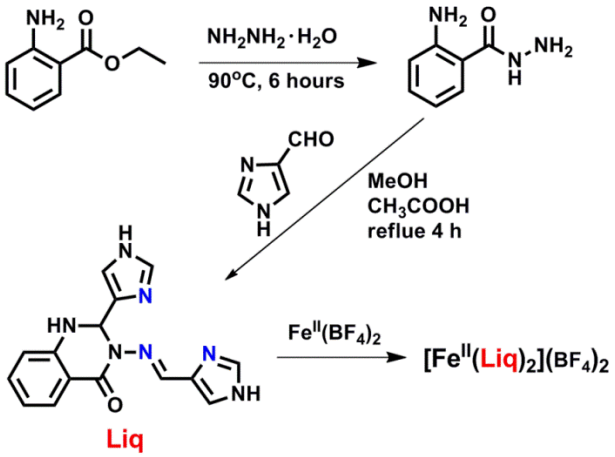

Scheme 1. Synthetic route to the new ligand Liq and its Fe^{II} complex reported in this Work

Experimental

Materials and General Procedures

All the reagents employed were commercially available and used without further purification. Methanol and acetonitrile were dried using standard procedures. Perdeuterated dimethyl sulfoxide (DMSO-d_6) was commercially obtained from Alfa Aesar Co. Ltd.

Elemental analyses (C, H, and N) were conducted with a Perkin-Elmer 2400 analyzer. Micro-IR spectroscopy studies were performed on a Nicolet Magna-IR 750 spectrophotometer in the 4000-400 cm^{-1} region (*w*, weak; *b*, broad; *m*, medium; *s*, strong) by KBr disc. ^{1}H NMR spectra were obtained from a solution in DMSO-d_6 using a Bruker-500 spectrometer. (*s*, singlet; *d*, doublet; *t*, triplet; *m*, multiplet; *dd*, double doublet). DSC measurement was performed on a TA DSC Q2000 instrument under nitrogen atmosphere at a scan rate of 5 K min^{-1} in both heating and cooling modes. TG analyses were recorded on a NETZSCH TG209F3 thermoanalyzer by being filled into alumina crucibles under N_2 atmosphere within the temperature range of 300−1000 K at a heating rate of 10 K min^{-1}. Cyclic voltammetry (CV) and differential pulse voltammetry (DPV) experiments were undertaken in acetonitrile (0.1 M $[Bu_4N](PF_6)$) at 293 ± 2 K using a CHI620E computer-controlled electrochemical workstation and a standard three-electrode cell. Glassy carbon microelectrode was used as the working electrode, whereas a platinum mesh and Ag/AgCl electrode were used as the counter and reference electrodes, respectively. All potentials given in this paper are referred to the ferrocene/ferrocenium ($[FeCp_2]^{0/+}$) reference couple under the same conditions.

Magnetic Measurements

Magnetic susceptibility measurements were performed using a Quantum Design MPMS XL-5 SQUID magnetometer. The magnetic susceptibility measurements were taken on a freshly prepared crystal sample wrapped in a polyethylene membrane to avoid any loss of solvent for magnetic measurements while lowering the temperature from 300 to 5 K at the sweeping rate of 1 K min^{-1} under an applied magnetic field of 2500 Oe. Corrections for diamagnetism were applied using Pascal's constants.

Table 1. Structure Refinement Parameters for Complexes **1**-Et_2O and **1**-$3H_2O$.

	1-Et_2O		**1-$3H_2O$**	
T/K	298(2)	123(2)	298(2)	123(2)
Formula	$C_{34}H_{36}B_2F_8FeN_{14}O_3$	$C_{34}H_{36}B_2F_8FeN_{14}O_3$	$C_{30}H_{32}B_2F_8FeN_{14}O_5$	$C_{30}H_{32}B_2F_8FeN_{14}O_5$
CCDC	1430792	1430791	1430794	1430793
FW	459.12	918.24	898.16	898.16
Crystal system	Orthorhombic	Orthorhombic	Orthorhombic	Orthorhombic
Space group	$P2_12_12$	$P2_12_12_1$	$P2_12_12_1$	$P2_12_12_1$
Flack parameter	0.022(15)	0.015(9)	0.03(4)	-0.003(13)
a (Å)	19.425(6)	9.2819(7)	9.4524(19)	9.3220(19)
b (Å)	9.389(3)	19.2352(14)	19.536(4)	19.465(4)
c (Å)	10.942(4)	21.4352(15)	21.598(4)	21.148(4)
V (Å^3)	1995.7(11)	3827.0(5)	3988.5(14)	3837.4(13)
Z	2	4	4	4
ρ_{calc}(g/cm)	1.528	1.594	1.496	1.555
μ (mm^{-1})	0.471	0.491	0.473	0.492
R_{int}	0.0603	0.0549	0.2422	0.0773
R_1,[a] $wR_2[I>2\sigma(I)]$	0.0840, 0.2182	0.0666, 0.1676	0.0850, 0.1979	0.0707, 0.1677
R_1, wR_2[all data]	0.1024, 0.2389	0.0900, 0.1852	0.2754, 0.2313	0.0909, 0.1853
GOOF[b]	1.031	1.157	0.603	1.020

[a] $R_1 = \Sigma||F_0| - |F_c||/\Sigma|F_0|$; $wR_2 = [\Sigma[w(F_0^2 - F_c^2)^2]/\Sigma[w(F_0^2)^2]]^{1/2}$.

[b] Goodness-of-fit = $[\Sigma[w(F_0^2 - F_c^2)^2]/(N_{obs} - N_{params})]^{1/2}$, based on the data $I>2\sigma(I)$.

Synthesis of compound 2-aminobenzhydrazide. It was synthesized according to the reported procedure with minor modification.[19] The combined solution of ethyl 2-aminobenzote (1.65 g, 10 mmol) and hydrazine hydrate (6.5 mL, 100 mmol) was refluxed for 6 hours. After the reaction was finished, the solution was left standing over night and 50 mL petroleum ether was added. The crude product was recrystallized from hot ethanol. Yields: 85%.

Synthesis of ligand Liq. A mixture methanol solution of 1H-Imidazole-4-carbaldehyde (0.9609 g, 10.0 mmol) and 2-aminobenzhydrazide (0.7559 g, 5.0 mmol) in presence of 0.2 mL glacial acetic acid was magnetically stirred for 4 hours at the boiling temperature, after cooling to room temperature, a pale yellow solid was obtained by filtration under reduced pressure. The crude product was washed with cold ethanol and dried in vacuo over P_2O_5. Yield: 91%. ^{1}H NMR (500 MHz, DMSO-d_6) δ 12.42(d, *J*=13.1, 1H), 11.92 (s, 1H), 8.72(s, 1H), 7.74(s, 1H), 7.69(dd, 1H), 7.54(s, 2H), 7.24(m, 1H), 6.82(s, 1H),

6.77(d, *J*=7.5, 1H), 6.76(t, 1H), 6.23(s, 1H) ppm. ^{13}C NMR (500MHz, DMSO-d_6): δ 161.45, 160.25, 147.58, 146.00, 139.53, 136.75, 134.89, 133.04, 127.51, 117.89, 116.70, 115.42, 114.53, 113.57, 67.84 ppm. IR(KBr pallet cm^{-1}): 517(w), 542(w), 607 (w), 620 (m), 700 (w), 720 (w), 748 (m), 782 (w), 822(w), 852(w), 933 (w), 955 (w), 987 (m), 1083(w), 1147(w), 1255(m), 1296(w), 1325(w), 1345(w), 1405(m), 1436(m), 1516(w), 1538(w), 1585(m), 1624(s), 2861(w), 3195(s). Anal. Calcd for $C_{15}H_{13}N_7O$: H, 4.26; C, 58.62; N, 31.91. Found: H, 4.19; C, 58.71; N, 31.83.

Preparation of compound [Fe(Liq)$_2$](BF$_4$)$_2$·(CH$_3$CH$_2$)$_2$O (1-Et$_2$O): A solution of $Fe(BF_4)_2\cdot 6H_2O$ (0.05 mmol, 16.85 mg) in MeCN (3 mL) was added to a solution of Liq (0.1 mmol, 30.71 mg) in MeCN (5 mL). The resulting dark-red mixture was stirred under nitrogen atmosphere for 1 hour. The suspension was then filtered and the filtrate was layered below diethyl ether in a tiny tube. Dark red block-shaped single crystals suitable for X-Ray diffraction analysis were obtained after several days. Yield: 51% (based on Fe). IR(KBr pallet cm^{-1}): 540(w), 616(w), 668(w), 751(m), 840.30(w), 993 (m), 1089 (s), 1159 (m), 1236(m), 1267(w), 1338(w), 1395(m), 1446(w), 1510(m), 1606(s), 1644(w), 2927(w), 3125(m), 3412(s). Anal. Calcd (%) for $[Fe(C_{15}H_{13}N_7O)_2](BF_4)_2\cdot(CH_3CH_2)_2O$: H, 3.95; C, 44.48; N, 21.36. Found(%): H, 3.88; C, 44.25; N, 21.03.

Preparation of compound [Fe(Liq)$_2$](BF$_4$)$_2$·3H$_2$O (1-3H$_2$O): The sample **1**-3H$_2$O was obtained by exposure of **1**-Et$_2$O in moisture under ambient condition for 2 weeks, in such case, the saturated amount of water in lattice, namely, three water molecules per host were at most adsorbed. IR(KBr pallet cm^{-1}): 533(w), 616(w), 689(w), 754(m), 785(w), 986(w), 1084(s), 1124 (m), 1154(m), 1232(w), 1274(w), 1342(m), 1388(w), 1506(m), 1611(s), 1652(m), 2927(w), 3122 (m), 3419(s). Anal. Calcd (%) for $[Fe(C_{15}H_{13}N_7O)_2](BF_4)_2\cdot 3H_2O$: H, 3.59; C, 40.12; N, 21.83. Found(%): H, 3.53; C, 40.72; N, 21.39. Since the single crystallinity was retained during the solvent exchange process in air, we were able to obtain the crystals suitable for X-ray diffraction analysis and refine the structure data of **1**-3H$_2$O successfully.

The crystal **1'**- Et$_2$O can be recovered by exposure of **1**-3H$_2$O in ether for several hours, which is evidenced by the element analysis (1'- Et$_2$O, found(%): H, 3.54; C, 44.12; N, 20.54) and magnetic susceptibility comparison with the data of as-synthesized **1**-Et$_2$O.

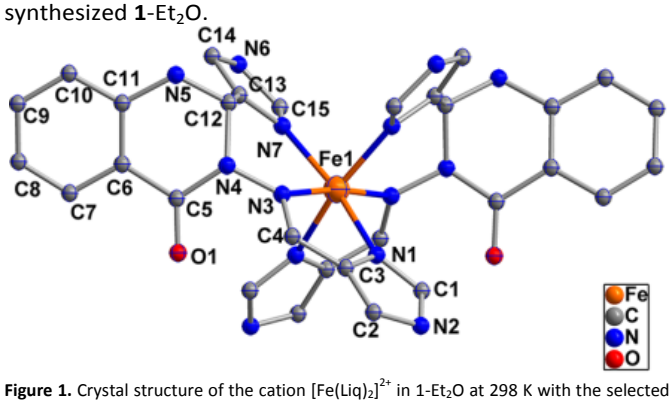

Figure 1. Crystal structure of the cation $[Fe(Liq)_2]^{2+}$ in 1-Et$_2$O at 298 K with the selected atom label. The anions and solvent molecules are omitted for clarity.

Results and discussion

Recrystallization of the pinkish solid obtained from 1:2 reactions of $Fe(BF_4)_2\cdot 6H_2O$ with Liq ligand in MeCN by vapor diffusion of ether gave rise to dark-red single crystals of $[Fe(Liq)_2](BF_4)_2\cdot(CH_3CH_2)_2O$ (**1**-Et$_2$O). The crystal **1**-Et$_2$O crystallized in orthorhombic chiral space group $P2_12_12$ at 298 K. (Table 1) The unit cell consists of half of the symmetry-related $[Fe(Liq)_2]^{2+}$ cations and one BF_4^- counteranion (Figure. 1). Each *mer*-tridentate Liq ligand coordinates to Fe(II) center equatorially *via* two imidazol donors and axially via the imine N atoms completing the coordination sphere. The value of *trans* N-(imidazol)−Fe−N(imidazol) angle [166.82°] together with another *trans* N_{azo}–Fe–N_{azo} angles [172.45°] reflect the steric constraints imposed by the rigidity of the tridentate imidazol ligand. The distortion parameter Σ equals 58.9(3)°.[22] The axial bond with the Fe–$N_{azomethine}$ lengths of 2.064(5) Å is comparable to the equatorial Fe–$N_{imidazol}$ averaged 2.050(9) and 2.078(5) Å (Table 2). It is worthy to note the bonding parameter in **1**-Et$_2$O, while smaller than typical Fe-N bond of 2.15 Å for high-spin Fe^{II}, are nevertheless larger than those expected for low-spin Fe^{II} centers, indicative of the intermediate spin state between HS and LS.

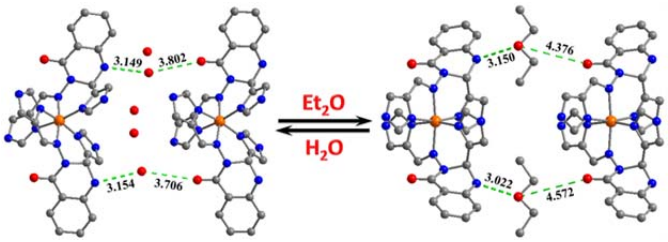

Figure 2. Reversible SCSC transformations between **1**-Et$_2$O, **1**-3H$_2$O (bottom) induced by guest exchange.

The unit cell measurements on an individual single crystal of **1**-Et$_2$O in the cooling mode from 298 K to 120 K were undertaken to observe the thermal-induced structure phase change. When the temperature was lowered to 120 K, at which the spin crossover is complete as indicated later, compound **1**-Et$_2$O crystallizes in another orthorhombic space group $P2_12_12_1$ with inverse *a* and *b* cell lengths and a doubling of the *c* axis and cell volume (Table 1). The asymmetric unit contains one entire molecule due to loss of the inversion symmetric element, revealing that the crystallographic phase change is possibly associated with spin-crossover. The variation of Fe–N and octahedral distortion parameter Σ are effective indicators for the occurrence of SCO (Table 2). Upon cooling to 120 K, the average axial/equatorial Fe–N bonds become obviously short and reach 1.969(6)/1.982(5) Å, characteristic of the low-spin Fe(II) site. In addition, Σ_{Fe} decreases to 44.2(2)°, in accordance with smaller Σ in the LS state and larger Σ in the HS state. The abundant hydrogen bonding interactions are involved between counteranions and imidazole nitrogen atoms (ESI, Figure S3, S5). The presence of N–H···F(anion) interactions in **1**-Et$_2$O will assist in the stabilization of a 2-dimensional supramolecular network along the [*ab*] plane. The neighbor supramolecular layer is further linked through the interlayer hydrogen bond association along the crystallographic *c* axis. In

addition, the O atom of solvent molecule (Et_2O) strongly interacts with nitrogen atom on dihydroquinazoline group through the N–H…O hydrogen bonding with D…A distance of 3.022/3.150 Å, which will aid to stabilize the ether molecule at high temperature (Figure 2). The presence of off-center parallel π–π stacking interactions along the *a*-axis between the dihydroquinazoline rings of two Liq ligands from two different $[Fe(Liq)_2]^{2+}$ units with a N3···N12 distance of 3.215 Å, as well as 3.707 Å between C5 and C26, gave rise to the short Fe···Fe distance of 9.282 Å at 120 K.

Table 2. Selected Interatomic Distances(Å) and Angles(deg) for **1**-Et_2O and **1**-$3H_2O$.

	1-Et_2O		1-$3H_2O$	
T(K)	123	298	123	298
Fe-N_{im1}	1.983(5)	2.052(6)	1.987(5)	1.973(4)
	1.998(5)	2.052(6)	1.998(5)	1.997(4)
Fe-$N_{im,\ avg}$	1.991(0)	2.052(6)	1.992(5)	1.985(4)
Fe-N_{im2}	1.981(5)	2.078(5)	1.973(5)	1.977(4)
	1.983(5)	2.078(5)	1.982(5)	2.012(4)
Fe-$N_{im,\ avg}$	1.982(5)	2.078(5)	1.978(0)	1.995(4)
Fe-N_{azom}	1.967(5)	2.064(5)	1.987(5)	1.962(5)
	1.972(5)	2.064(5)	1.998(5)	2.038(4)
Fe-$N_{azom,\ avg}$	1.969(6)	2.064(5)	1.993(0)	2.000(5)
Σ^a	44.2(2)	58.9(3)	42.0 (3)	48.3(17)

[a]The distortion parameter Σ is defined as the sum of the deviation from 90° of the 12 *cis* angles of the FeN_6 octahedron.

To investigate structures associated with different SCO phases identified by the magnetic studies (see below) before and after guest-induced SCSC transformation, single-crystal X-ray diffraction data were collected *in situ* on one crystal of **1**-Et_2O in a successive exposure to ambient air/ether cycle. Upon standing in air for two weeks, the ether guest molecules were removed and surprisingly SCSC transformation occurred from **1**-Et_2O to its hydration form, denoted as **1**-$3H_2O$, as shown in Figure 2. At room temperature, the relatively high R_1 and wR_2 values may be caused by the heavily disordered solvents but the diffraction data is sufficient to confirm connectivity. Fortunately, the high-quality single-crystal X-ray diffraction data were obtained when lowering the temperature to 120 K. **1**-$3H_2O$ crystallizes in a chiral space group $P2_12_12_1$, the average Fe-N bond lengths shrink from 2.062(3) Å in **1**-Et_2O to 1.993(3) Å in **1**-$3H_2O$, and Σ value also changed from 58.9(3) to 48.3(17)° for Fe1, suggesting that Fe^{II} ion is in a full LS state. When this sample was cooled to 120 K, unlike compound **1**-Et_2O, no crystallographic phase change was observed for **1**-$3H_2O$. The average Fe-N bond lengths and Σ values for Fe^{II} in **1**-$3H_2O$ (Table 2) varied only slightly from the corresponding values at room temperature, thus suggesting that the exchange of guest water molecules favors the stabilization of low-spin state. Two water molecules, i.e, O2w and O4w, link the neighboring Fe(II) cations into infinite 1-D chain along the crystallographic *c* axis through the dihydroquinazoline nitrogen and carboxylate oxygen in N…O…O H-bonding series with donor…accept distance of 3.154 (3.149) Å for N…O and 3.706 (3.802) Å for O…O in complex **1**-$3H_2O$. It is interesting that the hydrated crystal **1**-$3H_2O$ is able to re-exchange guest molecules and recover to the etherified form, **1**-Et_2O, by exposure to ambient ether vapor for several hours, indicative of reversible SCSC transformations along with guest exchange between ether and water molecules.

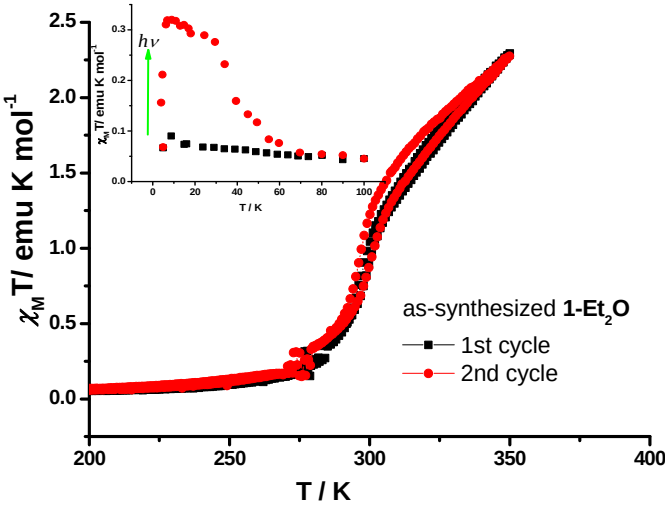

Figure 3. Variable-temperature magnetic susceptibility data of as–synthesized **1-Et_2O** and photo-induced magnetization (inset).

Thermogravimetry shows that desolvation is difficult to occur upon heating **1**-Et_2O. The mass loss with heating to *ca*. 108 °C accounts for the loss of all ether molecules (experimental: 8.4%, calculated 8.1 %). The de-solvated material is stable to 240 °C, beyond which temperature it decomposes (ESI, Figure S7). Magnetic susceptibility measurements have been performed on a freshly as-synthesized sample of $[Fe(Liq)_2](BF_4)_2{\cdot}(CH_3CH_2)_2O$ (**1**-Et_2O). The etherified form **1**-Et_2O were rapidly cooled to 100 K in SQUID apparatus and then measured upon at least two heating/cooling cycles. It is worth noting that no significant thermal hysteresis or irreversibility was observed when the temperature is cycled below 350 K despite partial ether molecules are removed from the solid in the SQUID magnetometer based on the TGA data. (The data up to 400 K, see supporting information, Fig S12) At lower temperature, the molecules correspond to low spin species, however, the χ_MT value abruptly increased to 1.04 cm^3 K mol^{-1} at 300 K and showed discontinuity in both cycles at *ca.* 275 K, which is associated with phase transition. (Figure. 3) Upon further warming, χ_MT values gently increase to 2.28 cm^3 K mol^{-1} at 350 K and SCO is still incomplete. In the subsequent cooling mode, χ_MT vs T curve is perfectly reproducible and no thermal hysteresis is observed. The second heating/cooling cycle produced a small thermal hysteresis loop, which is possibly related with the tiny solvent loss. The continuous heating-cooling cycles up to 400 K gave rise to the different

magnetic hysteresis loops, which was perhaps associated with the solvent-free phase in the SQUID holder under He atmosphere.(Figure S8, ESI) Thus, the etherfied sample undergoes a reversible SCO behavior with $T_{1/2}$ value of *ca*. 305 K.[23, 24]

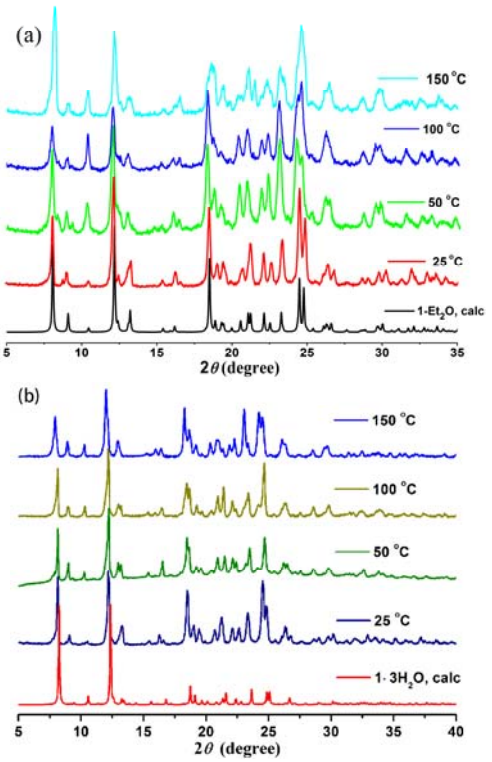

Figure 4. Variable temperature powder XRD patterns of the fresh ether sample **1**-Et_2O (a) and **1**-$3H_2O$ (b). The top line of (a) corresponds to the Et_2O-reabsorbed sample **1'**-Et_2O.

The hydrated sample can be obtained by exposing **1**-Et_2O in air for two weeks to allow full exchange of guest molecules. Element analysis is agreement with the single crystal X-ray diffraction data, which revealed three water molecules can be adsorbed per host at most.[26] After **1**-$3H_2O$ sample was exposed to ether vapor and allowed to reabsorb Et_2O in the lattice, the unit cell recovered to the one corresponding to the parent sample **1**-Et_2O. The data of **1**-$3H_2O$ and **1**-Et_2O were also checked by the powder XRD in Figure 4 to establish the structural integrity upon heating the samples despite the potential loss of partial solvent molecules.

The magnetic comparison revealed **1**-$3H_2O$ SCO property is significantly different from that of **1**-Et_2O, the magnetic susceptibility data revealed the diamagnetic character at room temperature (Figure. 5). The χ_MT value increases gradually to 0.4 cm^3 mol^{-1} K at 320 K, then abruptly to 2.79 cm^3 mol^{-1} K at 370 K, and then increases gradually to a final value of 3.22 cm^3 mol^{-1} K at 400 K. This curve indicates an SCO transition with $T_{1/2}\uparrow$ = 346 K. The subsequent cooling mode provides evidence for a 20 K hysteresis loop. Although the spin transition is accompanied by partial removal of solvent molecules from TG analysis, an additional heating/cooling cycle shows almost reproducibility and didn't significantly change the thermal hysteresis loop.[27] The spin and oxidation state of the Fe complex **1**-$3H_2O$ was further probed by Mössbauer spectroscopy (ESI, Figure S9), which shows an isomer shift of 0.30 mm s^{-1} and quadrupole splitting of 0.235 mm s^{-1} at 300 K, indicating the exclusive existence of a LS Fe(II) center at that temperature, a result which is consistent with the information obtained from X-ray diffraction analysis.[28] Furthermore, magnetic data comparison revealed the sample **1**-$3H_2O$ can be reversibly transformed to etherified sample **1**'-Et_2O. (ESI, Figure S10). On the basis of the single-crystal structures and magnetic data of **1**-Et_2O and **1**-$3H_2O$, the single-crystal-to-single-crystal transformation gives rise to the hysteresis "off-on" switching behavior due to the exchange of lattice solvent molecules.

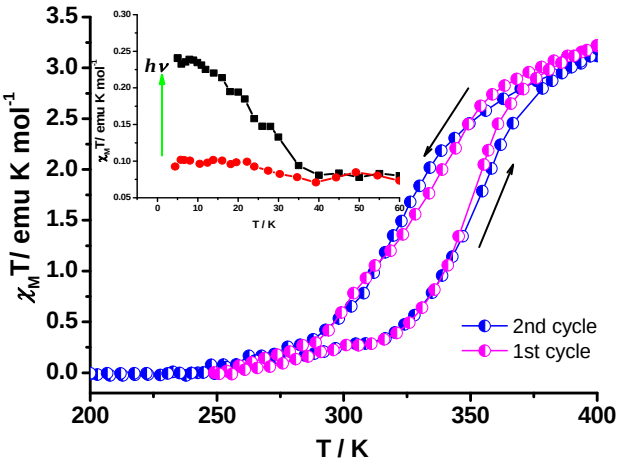

Figure 5. Variable-temperature magnetic susceptibility data of **1**-$3H_2O$, inset shows the photo-induced magnetization. The arrows indicate the heating or cooling mode in the measurements.

Photo-induced spin transition was further investigated on **1**-Et_2O and **1**-$3H_2O$, respectively, to differentiate the light induced excited spin state trapping (LIESST) effect.(inset of Figure 3 and Figure 5) After illumination with 532 nm light for 30 min at 5 K, the χ_MT product increased to 0.32 cm^3 K mol^{-1} and to 0.24 cm^3 K mol^{-1} to achieve almost saturation value for **1**-Et_2O and **1**-$3H_2O$, respectively, featuring spin transition from diamagnetic low spin to metastable high spin species. The efficiency of transition is far from being quantitative for **1**-Et_2O (10%) and hydrate analogue, **1**-$3H_2O$ (8%). The low transition efficiency is frequently associated with the short lifetime of LIESST state, in agreement with the original observations by Decurtins et al.[29] The relaxation temperature for **1**-Et_2O at 70 K is obviously higher than that for **1**-$3H_2O$ (40 K), which reveals that the etherified phase **1**-Et_2O should more stabilize the excited high spin state than hydration phase, consistent with the magnetic data at high temperature.

The solvent effect on the spin crossover property that may trigger the intermolecular cooperativity mainly includes the hydrogen bonding interaction,[30] the steric effect of the solvent,[31] and crystal symmetry of the solvate of complex. However, it seems obscure how the H-bonds influence the SCO transition temperatures. In some cases, authors suggest that stronger H-bonds can obviously weaken the ligand field, in favor of the HS states and lower transition temperature ($T_{1/2}$).[32] Conversely, the H-bonds in some cases can slightly increase the electron density on the amine/imine nitrogen of

the ligand, leading to the high transition temperature.[33] In our case, the transition temperature is lifted with the increasing hydrogen bonding. As for the influence of the H-bonds on the cooperativity, it was established that H bonds between the SCO active centers through the solvent molecules should efficiently transmit cooperativity and lead to more abrupt and/or wide hysteresis loops.[34] As for hydrated sample **1**-3H_2O, its SCO transition temperature is shifted higher than that of **1**-Et_2O. More interestingly, apparent hysteresis loop (20 K) was observed in the hydrated sample **1**-3H_2O, despite of the partial dehydration. The modification of H-bond interactions might be responsible for the amplification of thermal hysteresis. Through structure comparison between them, it was found that the water molecule as bridge smooth the strong intermolecular interaction. However, in complex **1**-Et_2O, this type of N…O…O hydrogen bonding series is blocked due to the weak donor ability of oxygen atom on ether guest by the distant O…O separation of 4.376 and 4.572 Å, respectively, which will weaken the intermolecular cooperativity.

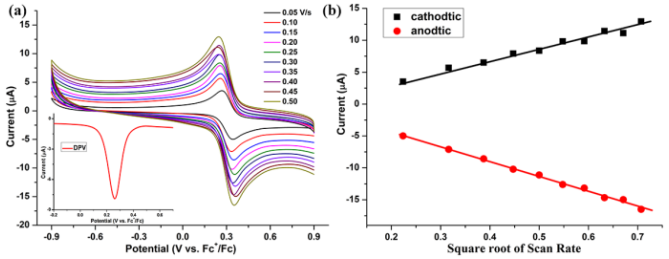

Figure 6. (a) Cyclic voltammograms at the different scan rate obtained in acetonitrile solution of **1-Et$_2$O**. Inset is the corresponding DPV data. (b) The linear relation between peak currents and the square root of the scan rates for complex **1-Et$_2$O**.

In order to test the stability and redox potential in solution, cyclic voltammograms (CV) and differential pulse voltammograms (DPV) were recorded for **1**-Et_2O (**Figure 6**). The electrochemical behavior of the compound shows a reversible redox signal with an obviously peak in the 0.2 to 0.4 V vs Fc^+/Fc interval. The electrochemically reversible process is diffusion-controlled, as evidenced by the linear dependence of both reduction and oxidation peak currents on the square root of the scan rate (**Figure 6b**). Deconvolution of these waves was attempted using DPV. These facts can be associated with predominant electronic effects, namely, the hard-base chelating character of the ligand donor, which strongly stabilizes the Fe^{II} oxidation state. From the observed electrochemical behavior, it can be asserted that the reduced species is very stable. Taken together, the voltammetric data establish the feature of Fe(II)↔Fe(III) reversible redox process, which potentially switch the molecule spin between S = 0 (Fe^{II}_{ls}) and S = 1/2 (Fe^{III}_{ls}).[35]

Conclusions

In conclusion, different solvate Fe^{II} complexes from the imidazole-bearing dihydroquinazoline tridentate donor providing strong ligand field were synthesized, structurally and magnetically characterized. X-ray diffraction revealed a reversible transformation between etherified form **1**-Et_2O and hydrate form **1**-3H_2O, which helps to understand the cooperativity difference. Magnetic studies indicated that **1**-Et_2O exhibit room temperature SCO behavior ($T_{1/2}$ = 305 K). The hydration moved the transition temperature and switched on an apparent thermal hysteresis. This finding emphasizes the importance of studying the solvation sensitive SCO magnetic properties of such materials and the interesting switching property of hysteresis around room temperature by reversible SCSC transformation, which is crucial to magnetic sensor and molecular switch.

Acknowledgements

We are thankful for financial support by the Priority Academic Program Development of Jiangsu Higher Education Institutions. This experimental work is financially funded by the NSFC program (Grants 21471023) and sponsored by Jiangsu Provincial QingLan Project. Wu thanks Prof. Y. Einaga's group in Keio University, Japan, for the data of Mössbauer spectra.

Notes and references

1 (a) O. Kahn and C. J. Martinez, *Science*, 1998, **279**, 44-48; (b) O. Kahn, J. Kröber and C. Jay, *Adv. Mater.*, 1992, **4**, 718-728; (c) S. Venkataramani, U. Jana, M. Dommaschk, F. D. Sönnichsen, F. Tuczek and R. Herges, *Science*, 2011, **331**, 445-448.

2 (a) A. Bousseksou, G. Molnar, L. Salmon and W. Nicolazzi, *Chem. Soc. Rev.*, 2011, **40**, 3313-3335; (b) E. Breuning, M. Ruben, J. M. Lehn, F. Renz, Y. Garcia, V. Ksenofontov, P. Gutlich, E. Wegelius and K. Rissanen, *Angew. Chem. Int. Ed.*, 2000, **39**, 2504-2507.

3 (a) M. A. Halcrow, *Chem. Soc. Rev.*, 2011, **40**, 4119-4142; (b) M. A. Halcrow, *Chem. Soc. Rev.*, 2008, **37**, 278-289; (c) J.F. Letard, P. Guionneau, E. Codjovi, O. Lavastre, G. Bravic, D. Chasseau and O. Kahn, *J. Am. Chem. Soc.*, 1997, **119**, 10861-10862; (d) M. A. Halcrow, *Coord. Chem. Rev.*, 2009, **253(21-22)**, 2493-2514.

4 I. Šalitroš, N. T. Madhu, R. Boča, J. Pavlik and M. Ruben, *Monatsh. Chem.* 2009, **140**, 695-733 and references therein.

5 O. Kahn, C. J. Martinez, *Science*, 1998, **279**, 44-48. (b) J. G. Haasnoot, *Chem. Soc. Rev.*, 2000, **200**, 131-185; (c) G. Aromi, L. Barrios, A. Leoni, O. Roubeau and P. Gamez, *Chem. Soc. Rev.*, 2011, **255**, 485-546; (d) M. H. Klingele and S. Brooker, *Chem. Soc. Rev.*, 2003, **241**, 119-132; (e) Y. Garcia, O. Kahn, L. Rabardel, B. Chansou, L. Salmon and J. P. Tuchagues, *Inorg. Chem.*, 1999, **38**, 4663-4670.

6 T. Delgado, A. Tissot, C. Besnard, L. Guenee, P. Pattison and A. Hauser, *Chem-Eur. J.*, 2015, **21**, 3664-3670. (b) H. J. Shepherd, C. Bartual-Murgui, G. Molnar, J. A. Real, M. C. Munoz, L. Salmon and A. Bousseksou, *New. J. Chem.*, 2011, **35**, 1205-1210; (c) J. Y. Li, Z. Yan, Z. P. Ni, Z. M. Zhang, Y. C. Chen, W. Liu and M. L. Tong, *Inorg. Chem.*, 2014, **53**, 4039-4046.

7 (a) T. M. Klapötke, P. Mayer, J. Stierstorfer and J. J. Weigand, *J. Mater. Chem.*, 2008, **18**, 5248-5258; (b) M. Friedrich, J. C. Gálvez-Ruiz, T. M. Klapötke, P. Mayer, B. Weber and J. J. Weigand, *Inorg. Chem.*, 2005, **44**, 8044-8052; (c) Y. B. Lu, M. S. Wang, W. W. Zhou, G. Xu, G. C. Guo and J. S. Huang, *Inorg. Chem.*, 2008, **47**, 8935-8942; (d) E. Q. Gao, N. Liu, A. L. Cheng and S. Gao, *Chem. Commun.*, 2007, 2470-2472.

8 C. Cook, F. Habib, T. Aharen, R. Clérac, A. Hu and M. Murugesu, *Inorg. Chem.*, 2013, **52**, 1825-1831.

9 D. Schweinfurth, S. Demeshko, S. Hohloch, M. Steinmetz, J. G. Brandenburg, S. Dechert, F. Meyer, S. Grimme and B. Sarkar, *Inorg. Chem.*, 2014, **53**, 8203-8212.

10 (a) L. Zhang, G. C. Xu, H. B. Xu, T. Zhang, Z. M. Wang, M. Yuan and S. Gao, *Chem. Commun.*, 2010, **46**, 2554-2556; (b) L. Zhang, J. J. Wang, G. C. Xu, J. Li, D. Z. Jia and S. Gao, *Dalton Trans.*, 2013, **42**, 8205-8208.

11 (a) R. Boca, M. Boca, L. Dlhan, K. Falk, H. Fuess, W. Haase, R. Jarosciak, B. Papankova, F. Renz, M. Vrbova and R. Werner, *Inorg. Chem.*, 2001, **40**, 3025-3033; (b) R. Boca, F. Renz, M. Boca, H. Fuess, W. Haase, G. Kickelbick, W. Linert and M. Vrbova-Schikora, *Inorg. Chem. Commun.*, 2005, **8**, 227-230; (c) Y. Bodenthin, G. Schwarz, Z. Tomkowicz, A. Nefedov, M. Lommel, H. Mohwald, W. Haase, D. G. Kurth and U. Pietsch, *Phys. Rev. B*, 2007, **76**, 064422; (d) G. S. Matouzenko, S. A. Borshch, E. Jeanneau and M. B. Bushuev, *Chem.–Eur. J.*, 2009, **15**, 1252-1260; (e) I. Salitro, J. Pavlik, R. Boca, O. Fuhr, C. Rajaduraia and M. Ruben, *Cryst. Eng. Comm*, 2010, **12**, 2361-2368; (f) G. Schwarz, Y. Bodenthin, Z. Tomkowicz, W. Haase, G. Thomas, J. Kohlbrecher, U. Pietsch and D. G. Kurth, *J. Am. Chem. Soc.*, 2011, **133**, 547-558.

12 (a) B. Weber, W. Bauer and J. Obel, *Angew. Chem. Int. Ed.*, 2008, **47**, 10098-10101; (b) R. Nowak, W. Bauer, T. Ossiander and B. Weber, *Eur. J. Inorg. Chem.*, 2013, 975-983; (c) C. Lochenie, W. Bauer, A. P. Railliet, S. Schlamp, Y. Garcia and B. Weber, *Inorg. Chem.*, 2014, **53**, 11563-11572; (d) S. Schönfeld, C. Lochenie, P. Thoma and B. Weber, *CrystEngComm*, 2015, **17**, 5389-5395.

13 S. Hayami, Z-Z. Gu, H. Yoshiki, A. Fujishima and O. Sato, *J. Am. Chem. Soc.*, 2001, **123**, 11644-11650.

14 (a) G. J. Halder, C. J. Kepert, B. Moubaraki, K. S. Murray and J. D. Cashion, *Science*, 2002, **298**, 1762-1765; (b) S. M. Neville, G. J. Halder, K. W. Chapman, M. B. Duriska, B. Moubaraki, K. S. Murray and C. J. Kepert, *J. Am. Chem. Soc.*, 2009, **131**, 12106-12108.

15 (a) V. Niel, A. L. Thompson, M. C. Munoz, A. Galet, A. E. Goeta and J. A. Real, *Angew. Chem. Int. Ed.*, 2003, **42**, 3760-3763; (b) T. Glaser, *Angew. Chem. Int. Ed.*, 2003, **42**, 5668-5670.

16 (a) G. J. Halder, C. J. Kepert, B. Moubaraki, K. S. Murray and J. D. Cashion, *Science*, 2002, **298**, 1762-1765; (b) R. J. Wei, J. Tao, R.-B. Huang and L. S. Zheng, *Inorg. Chem.*, 2011, **50**, 8553-8564.

17 (a) J. J. M. Amoore, C. J. Kepert, J. D. Cashion, B. Moubaraki, S. M. Neville and K. S. Murray, *Chem. Eur. J.*, 2006, **12**, 8220-8227; (b) M. Clemente-León, E. Coronado, M. C. Giménez-López and F. M. Romero, *Inorg. Chem.*, 2007, **46**, 11266-11276; (c) M. Nihei, L. Han and H. Oshio, *J. Am. Chem. Soc.*, 2007, **129**, 5312-5313; (d) B. Li, R. J. Wei, J. Tao, R. B. Huang, L. S. Zheng and Z. P. Zheng, *J. Am. Chem. Soc.*, 2010, **132**, 1558-1566; (e) A. D. Naik, K. Robeyns, C. F. Meunier, A. F. Léonard, A. Rotaru, B. Tinant, Y. Filinchuk, B. L. Su and Y. Garcia, *Inorg. Chem.*, 2014, **53**, 1263-1265; (f) J. S. Costa, S. Rodríguez-Jiménez, G. A. Craig, B. Barth, C. M. Beavers, S. J. Teat and G. Aromí. *J. Am. Chem. Soc.*, 2014, **136**, 3869-3874; (g) D. Gentili, N. Demitri, B. Schäfer, F. Liscio, I. Bergenti, G. Ruani, M. Ruben and M. Cavallini, *J. Mater. Chem. C*, 2015, **3**, 7836-7844.

18 K. B. Gudasi, R. S. Vadavi, R. V. Shenoy, M. S. Patil, S. A. M. Patil and Nethaji, *Transit. Metal. Chem.*, 2005, **30**, 661-668.

19 H. Galons, C. Cave, M. Miocque, P. Rinjard, G. Tran and P. Binet, *Eur.-J .Med. Chem.*, 1990, **25**, 785-788.

20 *SMART and SAINT*: Area Detector Control and Integration Software; Siemens Analytical X-ray Systems, Inc.: Madison, WI, 1996.

21 *SHELXTL V5.1*, Software Reference Manual; Bruker, AXS, Inc.:Madison, WI, 1997.

22 (a) P. Guionneau, M. Marchivie, G. Bravic, J.-F. Létard and D. Chasseau, *J. Mater. Chem.*, 2002, **12**, 2546-2551. (b) P. Guionneau, M. Marchivie, G. Bravic, J.-F. Létard and D. Chasseau, *Top. Curr. Chem.*, 2004, **234**, 97 and references cited therein.

23 $T_{1/2}$ is defined as the temperatures for which there are 50% high-spin and 50% low spin states. For full population of high spin, the $\chi_M T$ value is assumed to be 3.0 emu K mol^{-1}.

24 (a) O. Roubeau, M. Castro, R. Burriel, J. G. Haasnoot and J. Reedijk, *J. Phys. Chem. B*, 2011, **115**, 3003-3012; (b) Z. Arcis-Castíllo, S. Zheng, M. A. Siegler, O. Roubeau, S. Bedoui and S. Bonnet, *Chem.-Eur. J.* 2011, **17**, 14826-14836.

25 (a) S. Brooker, *Chem. Soc. Rev.*, 2015, **44**, 2880-2892. (b) R. Kulmaczewski, J. Olguín, J. A. Kitchen, H. L. C. Feltham, G. N. L. Jameson, J. L. Tallon and S. Brooker, *J. Am. Chem. Soc.*, 2014, **136**, 878-881.

26 In the attempt, it takes two weeks to adsorb water molecules to saturation amount, i.e. $3H_2O$ per Fe(II) complex.

27 (a) R. Kulmaczewski, H. J. Shepherd, O. Cespedes and M. A. Halcrow, *Inorg. Chem.*, 2014, **53**, 9809-9817; (b) Z. Yan, J.-Y. Li, T. Liu, Z.-P. Ni, Y.-C. Chen, F.-S. Guo and M.-L. Tong, *Inorg. Chem.*, 2014, **53**, 8129-8135.

28 (a) A. Bleuzen, V. Marvaud, C. Mathoniere, B. Sieklucka and M. Verdaguer, *Inorg. Chem.*, 2009, *48*, 3453-3466; (b) O. Sato, *Acc. Chem. Res.*, 2003, **36**, 692-700.

29 S. Decurtins, P. Gütlich, C. P. Köhler, H. Spiering and A. Hauser, *Chem. Phys. Lett.*, 1984, **105**, 1-4.

30 I. Nemec, R. Herchel and Z. Trávníček, *Dalton Trans.*, 2015, **44**, 4474-4484.

31 D. Chernyshov, M. Hostettler, K. W. Törnroos and H.-B. Bürgi, *Angew. Chem. Int. Ed.* 2003, **42**, 3825-3830.

32 G. Lemercier, N. Bréuel, S. Shova, J. A. Wolny, F. Dahan, M. Verelst, H. Paulsen, A. X. Trautwein and J.-P. Tuchagues, *Chem.-Eur. J.*, 2006, **12**, 7421-7432.

33 T. Buchen, P. Gütlich and H. A. Goodwin, *Inorg. Chem.*, 1994, **33**, 4573-4576.

34 M. Hostettler, K. W. Trnroos, D. Chernyshov, B. Vangdal and H.-B. Bürgi, *Angew. Chem. Int. Ed.*, 2004, **43**, 4589.

35 M. G. Cowan, J. Olguín, S. Narayanaswamy, J. L. Tallon and S. Brooker, *J. Am. Chem. Soc.*, 2012, **134**, 2892-2894.